Improvement of Microwave Metamaterial Aperture Imager with Genetic Algorithm

Shuncheng Tian and Long Li

Key Laboratory of High Speed Circuit Design and EMC of Ministry of Education
School of Electronic Engineering
Xidian University, Xi'an, 710071, China
sctian@xidian.edu.cn, lilong@mail.xidian.edu.cn

Abstract ─ The genetic algorithm is used to improve the imaging capability of the microwave metamaterial aperture imager operating at Ku-band. The microwave metamaterial aperture imager is made up of the complementary electric-LC elements and Jerusalem cross structures elements. Besides, the genetic algorithm is applied to optimize the array of the elements, which can reduce the average mutual coherence of the patterns of the microwave metamaterial aperture imager at different frequencies. Then, the patterns of the microwave metamaterial aperture imager is used for the image reconstruction experiments. From the image reconstruction results, it can be seen that the quality of the recovered image is improved. The performance of the microwave metamaterial aperture imager using the genetic algorithm is crucially enhanced and extensive simulations verify the effectiveness of the proposed improvement approaches.

Index Terms ─ Complementary electric-LC element, imager, genetic algorithm, metamaterial, quality-factor.

I. INTRODUCTION

The traditional imaging system is mainly based on the Nyquist sampling theorem. However, for this type of the imaging system, if we want to get a higher resolution image, we have to increase the sampling rate. As a result, a large amount of redundant data will be discarded in the process of data compression. Microwave metamaterial aperture imager (MMAI) is a novel imager system, which can generate forward looking image without using mechanical scanning or antenna arrays. The first MMAI system was proposed in [1]. The MMAI used a one-dimensional metamaterial aperture with an extremely wide frequency band to generate enough radiation fields to illuminate the target, and two-dimensional sparse targets in the scene can be reconstructed with an optimized compressed sensing (CS) algorithm as shown in Fig. 1. x and y represent the N×1 original image signal and the M×1 measurement image signal, respectively. A is the M×N measurement matrix, where M<<N. In [2], a 2D metamaterial aperture was verified to realize 3D imaging, and it was shown that by increasing the quality factor (Q-factor) of the metamaterial element, the image performance of MMAI could be improved. The potential of multisensor fusion by integrating an infrared structured-light and optical image sensor to accelerate the microwave was illustrated in [3]. In [4-5], different reconstruction algorithms were investigated, and the imaging performance could also be improved. In [6], a coherent computational imaging system was proposed which can utilize a sparse detector array of planar, frequency-diverse, metasurface antennas designed to operate over the W-band frequency range. In [7], a new approach for short-range wireless localization based on meta-aperture and compressed sensing (CS) was proposed. In [8], a reconfigurable, dynamic beam steering holographic metasurface aperture to synthesize a microwave camera at K-band frequencies was present.

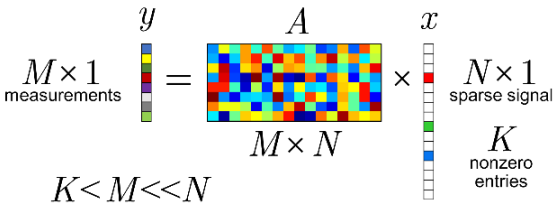

Fig. 1. Mathematical model of the CS algorithm.

For these methods above, the critical point is to ensure the non-correlative property between different measurement modes. From Fig. 2, it can been seen that the imaging performance is based on the radiation fields of the metamaterial aperture and the CS reconstruction algorithms. The information of the object can be obtained through repeating samples under different measurement modes. The performance of MMAI is mainly determined by the radiation field modes which provide enough measurements for the target. The common methods to increase the system radiation modes are to select the high Q-factor metamaterial resonant element and to design

Submitted On: December 1, 2018
Accepted On: July 10, 2019

MMAI in an extremely wide frequency bandwidth.

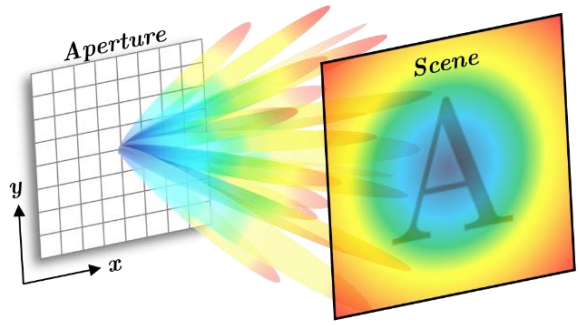

Fig. 2. Microwave metamaterial aperture imager system.

In the design of the metamaterial aperture, the non-correlative property converted to be the irrelevance of aperture's radiation characteristics under different frequencies changed in the work band to achieve much more measurements. The main contribution of this paper is the development of the higher frequency *Q*-factor CELC element and the random generation of the MMAI with the genetic algorithm. Specifically, Section II gives a brief introduction on the principles of MMAI. In Section III, a higher frequency *Q*-factor CELC element is analyzed. Section IV is devoted to the genetic algorithm on the design of the MMAI. Imaging experimental simulation results are given and discussed in Section V to demonstrate the effectiveness of the proposed design improvements on the MMAI. Finally, Section VI summarizes this work.

II. PRINCIPLE OF MMAI

In this section, the mathematical model of MMAI is briefly introduced. For the metamaterial aperture as an imaging system, a forward model must be implemented that describes how objects in the scene scatter the incident field, such that the collections by the receiver can be inverted and the scene will be retrieved. Though more sophisticated models can be developed, for our purposes the first born approximation provides a sufficient description. In this approximation, the field scattered from the target $\mathbf{E}_s$, is simply related to the incident field $\mathbf{E}_s$:

$$\mathbf{E}_s = \mathbf{E}_t f(\mathbf{r}), \tag{1}$$

where $f(r)$ is the target reflectivity at *r*. The scattered field propagating into the receiving probe antenna complies with the following proportionality:

$$y = \int \mathbf{E}_t(\mathbf{r})\mathbf{E}_s(\mathbf{r}) f(\mathbf{r}) d\mathbf{r}, \tag{2}$$

where *y* is the measurement of the scattered field collected by the receiving probe antenna. Considering the inherent frequency-diverse feature of complex radiation field, we can simplify (2) to:

$$y(\omega) = \int \mathbf{H}(\omega, \mathbf{r}) f(\mathbf{r}) d\mathbf{r}, \tag{3}$$

where $y(\omega)$ denotes the measurement of receiving probe at a certain driving frequency ω, $\mathbf{H}(\omega, \mathbf{r})$ is the measurement matrix, and the relationship between $\mathbf{E}_t(\mathbf{r})$ and $\mathbf{E}_s(\mathbf{r})$ can be calculated by:

$$\mathbf{H}(\omega, \mathbf{r}) = \mathbf{E}_t(\mathbf{r})\mathbf{E}_s(\mathbf{r}), \tag{4}$$

where $\mathbf{E}_t(\mathbf{r})$ and $\mathbf{E}_s(\mathbf{r})$ denote the fields from the transmitting metamaterial aperture and the receiving probe antenna projected to the point *r*, respectively. When the target information is reconstructed, its exact location is unknown. As a result, the scene is discretized into *N* voxels. If the frequency sweep is sampled at *M* frequency points, (3) becomes a finite dimension matrix equation as follows:

$$g_M = H_{M\times N} f_N, \tag{5}$$

where g_M is the received measurement matrix under a sequence of radiation field illumination varying with frequency, and f_N denotes the unknown reflectivities matrix of scene targets, and $H_{M\times N}$ is the measurement matrix whose k^{th} row elements corresponds to the complex field pattern at the driving frequency ω_k. Since the discretized pixels *N* is normally much larger than the number of measurement modes *M*, the linear equation in (5) can be extremely underdetermined, and it is difficult to solve (5) by the direct matrix inversion, thus the sophisticated CS technique is chose to estimate f_N with a promising solution.

III. COMPLEMENTARY ELECTRIC-LC (CELC) ELEMENT

For microwave metamaterial aperture imager system, the key is to increase the *Q*-factor of the metamaterial unit. That is to say, the unit must possess different center operating frequency and much narrower bandwidth in the operating frequency band of the metamaterial aperture. As pointed out by Hunt et al. [2], an increase in the *Q*-factor of the element for the metamaterial aperture causes the average mutual coherence μ to decrease, which indicates less correlation between measurements represents better orthogonality of the far-field patterns. Here the frequency *Q*-factor is defined as:

$$Q = f/BW, \tag{6}$$

where *f* and *BW* represent the center operating frequency and the frequency range in which the radiation efficiency decreases by half, respectively. If we want to recover images more accurately, the metamaterial aperture needs to work under more measurement modes in the limited operating frequency band. In other words, the *BW* of the metamaterial aperture unit needs to be much narrower and the frequency *Q*-factor will be even higher. In order to improve the frequency *Q*-factor, we select the following three methods in our work: 1) Use the asymmetric rectangular ring slot to instead the square ring slot because

the asymmetric structure can provide improvement on the frequency *Q*-factor; 2) Enlarge the period of the complementary electric-LC (CELC) element *P* while keep the size of the slot fixed, to raise the frequency *Q*-factor.

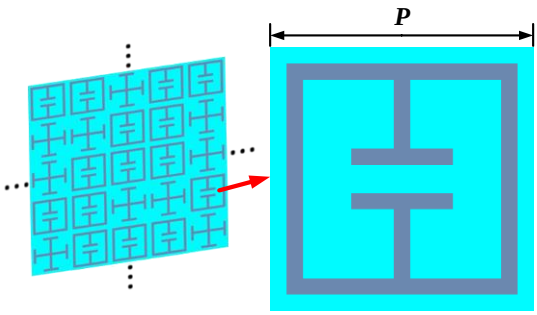

Fig. 3. Complementary electric-LC element.

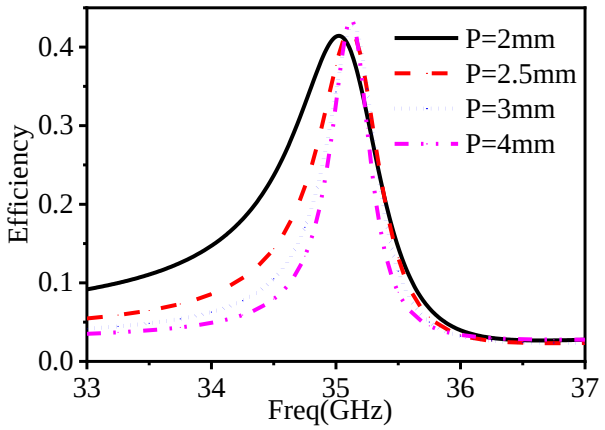

Fig. 4. Efficiency with different *P*.

Table 1: *Q*-factor of the CELC element with different *P*

***P* (*mm*)**	***Q*-factor**	***P* (*mm*)**	***Q*-factor**
2	37	3	70
2.5	58	4	86

By above ways, we could maximize the frequency diversity in the finite operating frequency band. In this paper, the improved the CELC element is proposed in Fig. 3. The CELC elements and Jerusalem cross structures elements with the proportion of 0.8 and 0.2, respectively. The higher *Q*-factor metamaterial cell is etched on the substrate upper plate and the bottom is the metal ground. Rogers 4350 is used with the dielectric constant of 3.66 and the thickness is 0.508*mm*. The proposed element is simulated with the infinite periodic boundary condition in HFSS. From Fig. 4, the *BW* of the metamaterial aperture unit can be narrowed by enlarging the period *P*. Meanwhile, if the dielectric constant is higher and the thickness is thinner, the *Q*-factor can also be enlarged. Because of the much smaller bandwidth, the number of measurement modes will be more in the same bandwidth, which makes it possible that more information can be obtained with the more different radiation features. As listed in Table 1, when *P*=4*mm*, the *Q*-factor is about 86, which means that the *Q*-factor of the novel CELC element can be improved by enlarging the period of the CELC unit.

As the operating frequency changes, the far-field radiation pattern of the MMAI changes. As pointed out by [9-10], when the bandwidth of the element becomes smaller, the average mutual coherence becomes much lower. As a result, the proposed higher *Q*-factor CELC element may realize to decrease the average mutual coherence μ to improve the imaging effect of the MMAI.

IV. THE GENETIC ALGORITHM ON THE DESIGN OF THE MMAI

Object within the scene scatters the incident fields and produce a backscattered field. In a transceiver configuration, the backscattered fields are detected by a single, low-gain waveguide probe with the same frequency. The low-gain waveguide probe ensures all the backscattered radiation field from object is collected as shown in Fig. 2. The MMAI system must obtain the detection ability in all the field of view (FOV) because the object may appear at any position in the scene. If the MMAI is made up of the CELC elements and Jerusalem cross structures elements randomly, which may lead to the result that the far field patterns of MMAI is not uniform distribution. As a result, the electromagnetic signals of the incident field cannot detect the object if the object is in the weak signals range in the FOV.

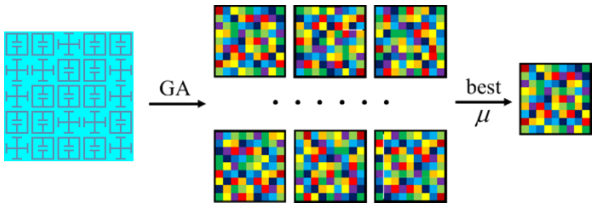

Fig. 5. Process of the genetic algorithm on the design of the MMAI.

In this section, the genetic algorithm (GA) is selected to assist to design the MMAI as shown in Fig. 5. The design process with the genetic algorithm can be summarize as follows:

1) Select the higher *Q*-factor CELC element with different sizes based on the element model base, determine the element amount and proportion of the higher *Q*-factor CELC element and Jerusalem Cross Unit; Initializatie the first population of the MMAI with different distributions and the cross mutation probability, take these MMAIs into the HFSS to simulate for the far field characteristics;

2) Take the simulation results of these MMAI into MATLAB to build the measurement matrix and compute the average mutual coherence μ; compare the average mutual coherence μ of different MMAIs and select some better MMAI with the lower μ as the new population;

3) Produce the novel MMAIs with the cross mutation operation based on the new population; repeat the simulation, computation μ, selection, production new population until the average mutual coherence not decrease.

Table 2: Average mutual coherence of different MMAIs

MMAI	Iteration Time		
	1	2	3
1	0.30704	0.29790	0.29945
2	0.31504	0.29819	0.29955
3	0.29964	0.30298	0.29589
4	0.29893	0.30088	0.29852
5	0.30562	0.29893	0.29790
6	0.30452	0.29964	0.29819
7	0.30024	0.30024	0.29893
8	0.31250	0.30452	0.29964
MMAI	**Iteration Time**		
	4	**5**	**6**
1	0.29790	0.29589	0.29589
2	0.29589	0.29589	0.29589
3	0.29819	0.29790	0.29589
4	0.29852	0.29790	0.29589
5	0.29589	0.29589	0.29589
6	0.29790	0.29589	0.29589
7	0.29819	0.29790	0.29589
8	0.29852	0.29790	0.29589

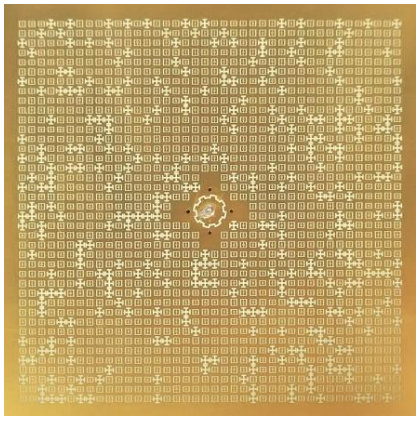

Fig. 6. Microwave metamaterial aperture.

With the properties of high Q-factor and frequency agility characteristic, the far-field pattern is different at different frequency because only a few elements mainly work at it particular frequency in the operating band. With the feature, the MMAI can be used in the imaging system. Finally, the measurement matrix A is set up by the use of the far-field patterns at different frequencies. The operating frequency range of the MMAI is set from 33GHz to 37GHz. In our work, eight MMAIs with different element distributions are selected as the initial population and optimized with the genetic algorithm. From the results in Table 2, when the iteration time reaches 6, the average mutual coherence of these MMAIs decreases to 0.29589, which verifies the effectiveness of the optimization on the MMAI design with the genetic algorithm.

V. IMAGE RECONSTRUCTION EXPERIMENTS

The MMAI is made up of 80% higher Q-factor metamaterial elements and 20% Jerusalem Cross elements as shown in Fig. 6. The far field patterns of the MMAI at 33GHz, 35GHz and 37GHz are described in Fig. 7, Fig. 8 and Fig. 9, respectively.

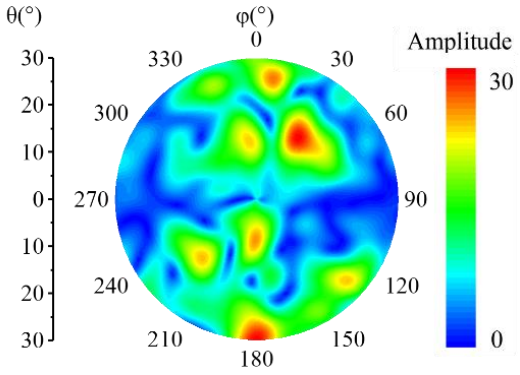

Fig. 7. Far field radiation patterns at 33GHz.

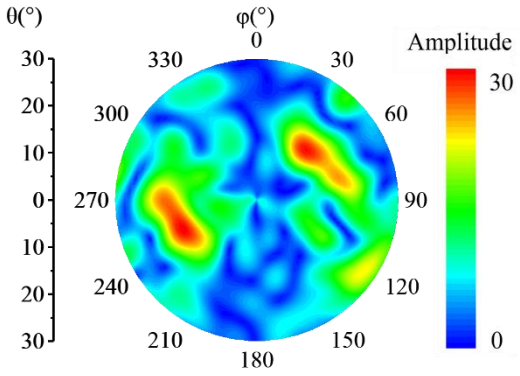

Fig. 8. Far field radiation patterns at 35GHz.

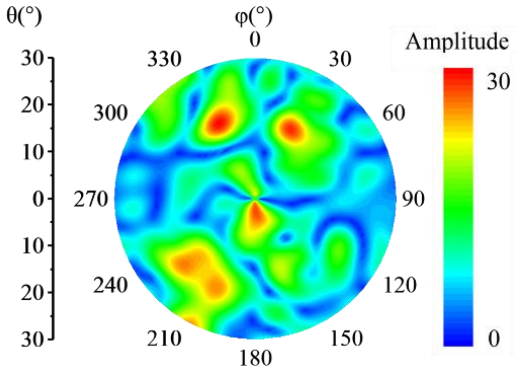

Fig. 9. Far field radiation patterns at 37GHz.

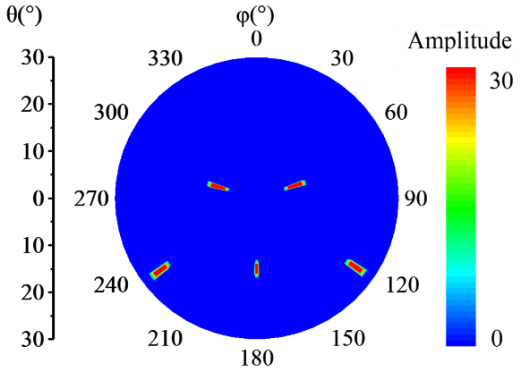

Fig. 10. The original image with five points.

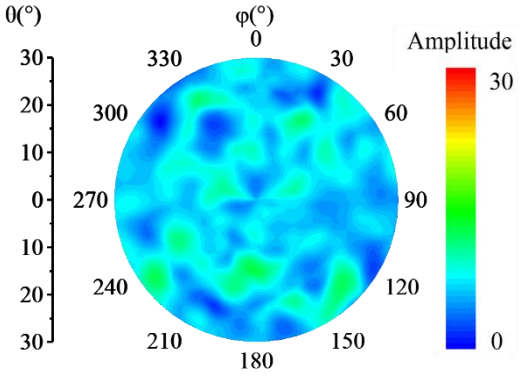

Fig. 11. Image reconstruction with the original MMAI.

The far field patterns can be used to build the measurement matrix to verify the feasibility of the MMAI. The optimized MMAI is used for the image reconstruction experimental simulations in Matlab. The goal of reconstruction is to estimate the set of target fractional scattering coefficients using the simulated measurement matrix. For the metamaterial-based frequency-diverse MMAI of consideration here, the number of available measurement modes can be significantly smaller than the number of voxels to be estimated according to compressed sensing theory.

To accomplish this goal, we discretize the scene into N voxels. Given the appropriate parameter for the reconstruction, it is in our interest to compare the image reconstruction effects with the measurement matrix of different average mutual coherences. The original image, in Fig. 10, is segmented into 31×361 blocks. The five red blocks is set as the object and the blue blocks is the background. Then, the restored image x can be calculated by $y=Ax$. x and y represent the $N\times1$ original image signal and the $M\times1$ received image signal, respectively. These image reconstruction experiments are done on a PC with Intel Xeon CPU E3-1230. Figure 11 and Fig. 12 give the image reconstruction of a simple target with two MMAIs with the average mutual coherence μ=0.35104 and μ=0.29589, respectively. Interestingly, the image reconstructed with the MMAI of the lower average mutual coherence has better quality than the higher μ MMAI. Through imaging experiments, the correctness and feasibility of the approaches proposed in this paper have been verified.

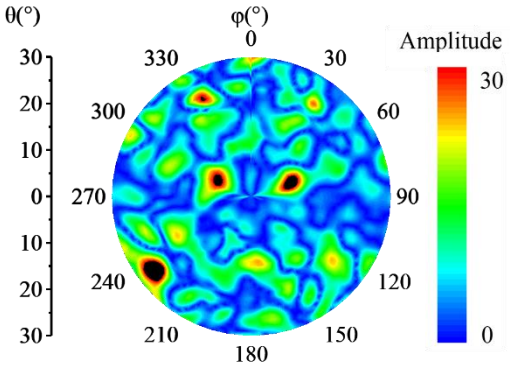

Fig. 12. Image reconstruction with the improved MMAI.

VI. CONCLUSION

An imaging system using dynamic MMAI has great potential in various applications. In particular, MMAI can overcome the complications of using complex hardware systems or moving parts. As such, a higher Q-factor metamaterial element is proposed to be applied in the imaging system, which holds a good frequency agility property. The bandwidth of it is much narrower than the common metamaterial element. Besides, by using the genetic algorithm, a lot of MMAIs is designed and simulated to produce the best one. The far field radiation patterns at different frequencies are used to construct suitable deterministic measurement matrix and improve the accuracy of image reconstruction. Then, the image reconstruction simulations are done to verify the correctness of the proposed approaches. The combination of a dynamic MMAI with reconstruction algorithm can lead to an imaging system that is efficient

and simple on the hardware and software levels. This exciting prospect opens the door to new opportunities in various research areas such as high-resolution, real-time, volumetric imaging.

ACKNOWLEDGMENT

This work is supported by National Natural Science Foundation of China under Contract No. 51477126, and supported by Technology Explorer and Innovation Research Project, and Fundamental Research Funds for the Central Universities (K5051202051 and SPSZ021409).

REFERENCES

[1] J. Hunt, T. Driscoll, A. Mrozack, G. Lipworth, M. Reynolds, D. Brady, and D. R. Smith, "Metamaterial apertures for computational imaging," *Science*, vol. 339, no. 6117, pp. 310-313, Jan. 2012.

[2] G. Lipworth, A. Mrozack, J. Hunt, D. L. Marks, T. Driscoll, D. Brady, and D. R. Smith, "Metamaterial apertures for coherent computational imaging on the physical layer," *Journal of the Optical Society of America A*, vol. 30, no. 8, pp. 1603-1612, Aug. 2013.

[3] J. Hunt, J. Gollub, T. Driscoll, G. Lipworth, A. Mrozack, M. Reynolds, D. J. Brady, and D. R. Smith, "Metamaterial microwave holographic imaging system," *Journal of the Optical Society of America A*, vol. 31, no. 10, pp. 2109-2119, Oct. 2014.

[4] O. Yurduseven1, M. F. Imani, H. Odabasi, J. Gollub, G. Lipworth, A. Rose, and D. R. Smith, "Resolution of the frequency diverse metamaterial aperture imager," *Progress In Electromagnetics Research*, vol. 150, pp. 97-107, Jan. 2015.

[5] G. Lipworth, A. Rose, O. Yurduseven, V. R. Gowda, M. F. Imani, and H. Odabasi, "Comprehensive simulation platform for a metamaterial imaging system," *Applied Optics*, vol. 54, no. 31, pp. 9343-53, Nov. 2015.

[6] T. Zvolensky, J. N. Gollub, D. L. Marks, and D. R. Smith, "Design and analysis of a w-band metasurface-based computational imaging system," *IEEE Access*, vol. 5, pp. 9911-9918, May 2017.

[7] T. Zhou, H. Li, D. Ye, J. Huangfu, S. Qiao, Y. Sun, W. Zhu, C. Li, and L. Ran, "Short-range wireless localization based on meta-aperture assisted compressed sensing," *IEEE Transactions on Microwave Theory and Techniques*, vol. 65, no. 7, pp. 2516-2524, Jan. 2017.

[8] O. Yurduseven, D. L. Marks, T. Fromenteze, and D. R. Smith, "Dynamically reconfigurable holographic metasurface aperture for a mills-cross monochromatic microwave camera," *Optics Express*, vol. 26, no. 5, pp. 5281-5291, Mar. 2018.

[9] N. Kou, L. Li, and S. Tian "Measurement matrix analysis and radiation improvement of metamaterial aperture antenna for coherent computational imaging," *Applied Science*, vol. 7, no. 9, p. 933, Sep. 2017.

[10] Z. Wu, Z. Lei, H. Liu, and N. Kou, "Range decoupling algorithm for accelerating metamaterial apertures-based computational imaging," *IEEE Sensors Journal*, vol. 18, no. 9, pp. 3619-3631, Mar. 2018.

Shuncheng Tian was born in Tianjin, China, in 1990. He received the B.E. degree from Xidian University, Xi'an, China, in 2013. He is currently pursuing the Ph.D. degree in Electromagnetic Fields and Microwave Technology at Xidian University, Xi'an, China.

His research interests include reflectarray analysis, frequency-selective surface analysis and design, automated neural network model generation algorithm, and electromagnetic field simulation and optimization.

Long Li (M'06–SM'11) was born in Guizhou Province, China. He received the B.E. and Ph.D. degrees in Electromagnetic Fields and Microwave Technology from Xidian University, Xi'an, China, in 1998 and 2005, respectively.

He was a Senior Research Associate with City University of Hong Kong, in 2006. He received the Japan Society for Promotion of Science (JSPS) Postdoctoral Fellowship and visited Tohoku University, Sendai, Japan, as a JSPS Fellow from November 2006 to November 2008. He was a Senior Visiting Scholar with the Pennsylvania State University, State College, PA, USA, from December 2013 to July 2014. He is currently a Professor with the School of Electronic Engineering, Xidian University. He is also the Director of Key Lab of High Speed Circuit Design and EMC, Ministry of Education, China. His research interests include metamaterials, electromagnetic compatibility, novel antennas, OAM, and wireless power transfer and harvesting technology.

Li was the recipient of the Nomination Award of National Excellent Doctoral Dissertation of China in 2007. He was also the recipient of the Program for New Century Excellent Talents in the University of the Ministry of Education of China in 2010, the First Prize of Awards for Scientific Research Results offered by Shaanxi Provincial Department of Education, China, in 2013, the IEEE APS Raj Mittra Travel Grant Senior Researcher Award in 2015, and the Shaanxi Youth Science and Technology Award in 2016.